Organometallics **1994,** *13,* 619–630

Borole Derivatives. 20.[1] Three-Center Fe–H–B Bonding in (Borole)(cyclopentadienyl)hydridoiron Derivatives

Gerhard E. Herberich,* Tobias Carstensen, Dieter P. J. Köffer, and Norbert Klaff

Institut für Anorganische Chemie, Technische Hochschule Aachen,
Professor-Pirlet-Strasse 1, D-52056 Aachen, Germany

Roland Boese

Institut für Anorganische Chemie, Universität-GH Essen,
Universitätsstrasse 3-5, D-45117 Essen 1, Germany

Isabella Hyla-Kryspin and Rolf Gleiter*

Institut für Organische Chemie der Universität Heidelberg,
Im Neuenheimer Feld 270, D-69120 Heidelberg, Germany

Martin Stephan

Institut für Anorganische Chemie der Universität Heidelberg,
Im Neuenheimer Feld 270, D-69120 Heidelberg, Germany

Helmut Meth and Ulrich Zenneck*

Institut für Anorganische Chemie der Universität Erlangen-Nürnberg,
Egerlandstrasse 1, D-91058 Erlangen, Germany

Received July 26, 1993[⊗]

(Borole)tricarbonyliron complexes $Fe(CO)_3(3,4\text{-}R^1_2C_4H_2BPh)$ (**3a**, $R^1 = H$; **3b**, $R^1 = Me$) react with cyclopentadiene under irradiation to give the hydrides $CpFeH(3,4\text{-}R^1_2C_4H_2BPh)$ (**1a**,**b**). Deprotonation by NaH in THF produces the borataferrocene anions $[CpFe(3,4\text{-}R^1_2C_4H_2BPh)]^-$ (**5a**$^-$, **5b**$^-$). These can be alkylated in the 2-/5-position by alkyl iodides in the presence of NaH to give 2,5-dialkyl hydride derivatives: e.g. $CpFeH(2,5\text{-}R^2_2C_4H_2BPh)$ (**1c**, $R^2 = Me$; **1g**, $R^2 = CH_2{=}CH(CH_2)_4$; **1h**, $R^2 = (CH_2)_2CHCH_2$). The structures of $CpFeH(2,3,4,5\text{-}Me_4C_4BPh)$ (**1d**; Fe–B = 215.1(4) pm, Fe–H = 147(3) pm, B–H = 151(3) pm) and $(C_5H_4Me)FeH(2,5\text{-}Me_2C_4H_2BPh)$ (**1f**; Fe–B = 215.5(2) pm, Fe–H = 147.5(23) pm, B–H = 146.1(26) pm) as determined by low-temperature X-ray diffraction show the presence of an Fe—H—B three-center bond with a weak B—H interaction. In solution **1a** establishes a mobile equilibrium between the ground state **1a-G** with Fe—H—B three-center bonding and the agostic isomer **1a-A** with Fe—H—C-2(C_4H_4B) three-center bonding with an estimated $\Delta G = 1.4$ kcal/mol. The hydridic proton and the 2-/5-protons of the borole ring undergo fast intramolecular exchange ($T_c = 333$ K at 80 MHz and $\Delta G^{\ddagger}_{333} = 17.0 \pm 0.7$ kcal/mol for **1a**). A merry-go-round of the three H atoms involved with one hydrogen crossing the exo face of the borole ligand is proposed as an exchange mechanism. The bonding in $CpFeH(C_4H_4BH)$ is analyzed by means of extended Hückel calculations, which confirm the Fe—H—B three-center bonding. Exploratory extended Hückel calculations also support the existence of agostic isomers as well as the proposed exchange mechanism. Cyclic voltammetry revealed the existence of the 17e complex $CpFe(C_4H_4BPh)$ (**5a**), which is characterized by its EPR and paramagnetic ^1H NMR spectra. **1a** reacts with $CNBu^t$ to give the boracyclopentenyl complex $CpFe(CNBu^t)(C_4H_5BPh)$ (**9a**) and, probably via the intermediate $Fe(CNBu^t)(C_4H_4BPh)(C_5H_6)$ (**10**), the borole complex $Fe(CNBu^t)_3(C_4H_4BPh)$ (**11a**) and 1 equiv of cyclopentadiene. Labeling experiments show that the shift of the hydridic hydrogen to the borole and Cp ligands, respectively, is an intramolecular process. **1c** reacts analogously.

Introduction

A great number of metal borole complexes, including triple-decker compounds, have been described in recent years.[1,2] While the chemistry of the borole ligand is well established, free 1*H*-boroles are highly reactive four-π-electron systems[3–6] and only a few sterically protected derivatives have been isolated to date.[5,6] Qualitative MO considerations show that the borole system possesses a diene-like HOMO and a low-lying LUMO. These properties favor transition-metal complexes with strong metal-to-ligand back-bonding. Anionic complexes, e.g. $[RhL_2]^-$,[7]

[⊗] Abstract published in *Advance ACS Abstracts,* January 1, 1994.

[1] Part 19: Herberich, G. E.; Carstensen, T.; Englert, U. *Chem. Ber.* **1992,** *125,* 2351.

[2] (a) Reference 1 and references quoted therein. (b) Herberich, G. E.; Köffer, D. P. J.; Peters, K. M. *Chem. Ber.* **1991,** *124,* 1947 and references quoted therein. (c) Hong, F.-E.; Fehlner, T. P.; Rheingold, A. L. *Organometallics* **1991,** *10,* 1213. (d) Sebald, A.; Wrackmeyer, B. *J. Organomet. Chem.* **1986,** *304,* 271.

[3] Herberich, G. E.; Ohst, H. *Chem. Ber.* **1985,** *118,* 4303.

0276-7333/94/2313-0619$04.50/0

Scheme 1

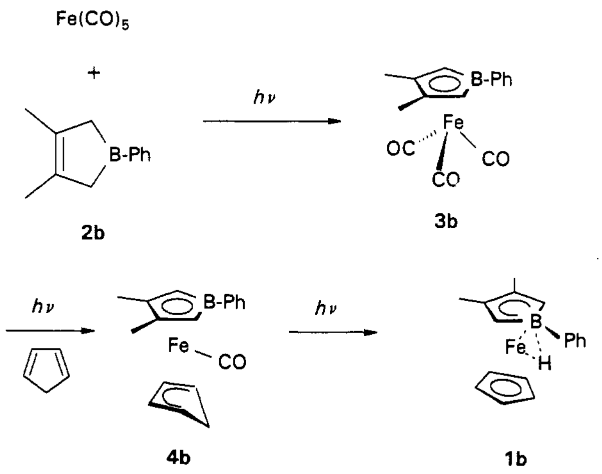

[CoL$_2$]$^-$,[8] [CpFeL]$^-$,[9] [LRe(CO)$_3$]$^-$,[10] [LFeH(CO)$_2$]$^-$,[11] and [LCo(CO)$_2$]$^-$ [1] (L = C$_4$H$_4$BPh), show only poor basicity (the Co and Rh systems with two borole ligands exist in neutral aqueous solution) owing to delocalization of the negative charge by back-bonding. As far as first-row transition-metal complexes are concerned, the corresponding hydrides often possess unusual nonclassical properties. In this paper we describe the synthesis and reactivity of the (borole)(cyclopentadienyl)iron hydrides **1** and of the corresponding anions. The structural problems associated with the hydrides **1**, both in the crystalline state and in solution, are addressed in detail.

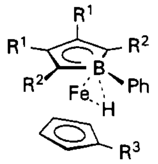

1a: R^1, R^2, R^3 = H[9]
b: R^1 = Me; R^2, R^3 = H
c: R^1 = H; R^2 = Me; R^3 = H
d: R^1, R^2 = Me; R^3 = H
e: R^1, R^2 = H; R^3 = Me
f: R^1 = H; R^2, R^3 = Me
g: R^1 = H; R^2 = CH$_2$=CH(CH$_2$)$_4$; R^3 = H
h: R^1 = H; R^2 = (CH$_2$)$_2$CHCH$_2$; R^3 = H

Results

Syntheses. The synthesis of **1a** has been reported previously.[9] The derivatives **1b**,**e** were made by the same route, which is summarized in Scheme 1. For the preparation of **1b** the 3,4-dimethylborolene species **2b**[12] is treated with Fe(CO)$_5$ under irradiation. The ensuing dehydrogenative complex formation[13] affords the borole complex **3b**. In the presence of cyclopentadiene this complex **3b** readily undergoes photochemical substitution to produce the monocarbonyl diene derivative **4b**, which, on prolonged irradiation, forms the hydride **1b**.

Scheme 2

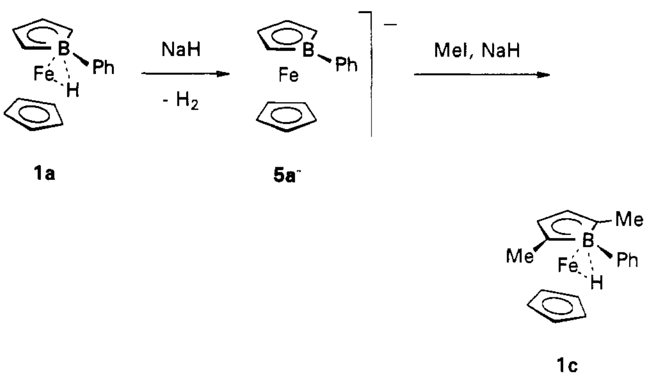

The hydrides **1a**,**b**,**e**, which do not carry substituents at the 2-/5-position of the borole ring, are very air-sensitive red solids with a characteristic smell. Pure samples could be stored under inert gas for several months. However, traces of impurities can cause spontaneous decomposition even at −30 °C. Contact with excess D$_2$O effects instantaneous H/D exchange of the hydrogen atoms at the iron and, surprisingly, at the 2-/5-position of the borole ligand; this process affords, e.g., **1a**-d_3.

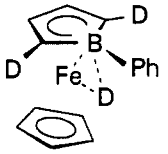

1a-d_3

The hydridic hydrogen is readily removed by NaH, yielding sodium salts of borataferrocene anions **5a**$^-$, **5b**$^-$, and **5e**$^-$. **5a**$^-$ has previously been characterized as the [Li(TMEDA)]$^+$ salt.[9] The anions **5a**$^-$, **5b**$^-$, and **5e**$^-$ react with methyl iodide in the presence of excess NaH to afford the 2,5-dimethylated hydride complexes **1c**,**d**,**f** (Scheme 2).

Monitoring the methylation by NMR spectroscopy shows that the monomethyl derivatives cannot be made selectively because of proton exchange between the various anionic and hydridic species in the reaction mixture. This exchange is fast even at −80 °C. Radical clock reagents[14] such as 1-iodo-5-hexene and (iodomethyl)cyclopropane produce the unrearranged products **1g**,**h** exclusively. This observation suggests that the alkylation proceeds via a straightforward S$_N$2 mechanism. Once the 2-/5-positions are alkylated, further alkylation is blocked.

---

(4) Fagan, P. J.; Burns, E. G.; Calabrese, J. C. *J. Am. Chem. Soc.* **1988**, *110*, 2979.

(5) (a) Eisch, J. J.; Galle, J. E.; Kozima, S. *J. Am. Chem. Soc.* **1986**, *108*, 379. (b) Herberich, G. E.; Buller, B.; Hessner, B.; Oschmann, W. *J. Organomet. Chem.* **1980**, *195*, 253. (c) Eisch, J. J.; Galle, J. E.; Shafii, B.; Rheingold, A. L. *Organometallics* **1990**, *9*, 2342.

(6) Sebald, A.; Wrackmeyer, B. *J. Organomet. Chem.* **1986**, *307*, 157.

(7) Herberich, G. E.; Büschges, U.; Hessner, B.; Lüthe, H. *J. Organomet. Chem.* **1986**, *312*, 13.

(8) Herberich, G. E.; Hessner, B.; Saive, R. *J. Organomet. Chem.* **1987**, *319*, 9.

(9) Herberich, G. E.; Hessner, B.; Köffer, D. P. J. *J. Organomet. Chem.* **1989**, *362*, 243.

(10) Herberich, G. E.; Dunne, B. J.; Hessner, B. *Angew. Chem.* **1989**, *101*, 798; *Angew. Chem., Int. Ed. Engl.* **1989**, *28*, 737.

(11) Herberich, G. E.; Carstensen, T.; Klaff, N.; Neuschütz, M. *Chem. Ber.* **1992**, *125*, 1801.

(12) (a) Söhnen, D. Dissertation, RWTH Aachen, 1984. (b) Herberich, G. E.; Boveleth, W.; Hessner, B.; Hostalek, M.; Köffer, D. P. J.; Ohst, H.; Söhnen, D. *Chem. Ber.* **1986**, *119*, 420.

(13) Herberich, G. E.; Boveleth, W.; Hessner, B.; Köffer, D. P. J.; Negele, M.; Saive, R. *J. Organomet. Chem.* **1986**, *308*, 153.

(14) (a) Newcomb, M.; Curran, D. P. *Acc. Chem. Res.* **1988**, *21*, 206. (b) Newcomb, M.; Glenn, A. G. *J. Am. Chem. Soc.* **1989**, *111*, 275. (c) Bowry, V. W.; Lusztyk, J.; Ingold, K. U. *J. Am. Chem. Soc.* **1991**, *113*, 5687. (d) Organometallic radicals such as CoCp$_2$ and CpFe(C$_6$Me$_6$) undergo extremely fast addition reactions with aliphatic radicals: Herberich, G. E.; Carstensen, T.; Klein, W.; Schmidt, M. U. *Organometallics* **1993**, *12*, 1439.

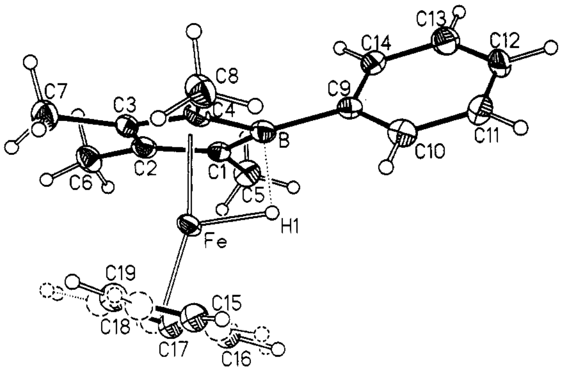

Figure 1. Presentation of the molecular structure (50% ellipsoids) of $CpFeH(C_4Me_4BPh)$ (**1d**).

Table 1. Atomic Coordinates of Non-Hydrogen Atoms and of the Hydridic Hydrogen Atom for 1d

atom	*x*	*y*	*z*	U_{eq}
Fe	0.6886(1)	0.6650(1)	0.0499(1)	19(1)^a
H	0.6431(12)	0.6818(12)	−0.0180(42)	36(10)^a
B	0.6287(1)	0.6318(1)	−0.0673(5)	21(1)^a
C1	0.6768(1)	0.6252(1)	−0.1609(4)	19(1)^a
C2	0.7097(1)	0.06020(1)	−0.0577(5)	20(1)^a
C3	0.6886(1)	0.5922(1)	0.0976(4)	19(1)^a
C4	0.06407(1)	0.06094(1)	0.1101(4)	19(1)^a
C5	0.6894(1)	0.6418(1)	−0.3283(4)	27(1)^a
C6	0.7595(1)	0.5871(1)	−0.1045(5)	26(1)^a
C7	0.7140(1)	0.5682(1)	0.2345(5)	27(1)^a
C8	0.6101(1)	0.6057(1)	0.2495(4)	29(1)^a
C9	0.5773	0.6434	−0.1435	20(1)^{a,b}
C10	0.5459(1)	0.6755(1)	−0.0705(2)	27(1)^{a,b}
C11	0.5015	0.6844	−0.1407	32(1)^{a,b}
C12	0.4886	0.6613	−0.2839	34(1)^{a,b}
C13	0.5200	0.6293	−0.3569	33(1)^{a,b}
C14	0.5643	0.6203	−0.2866	24(1)^{a,b}
C15	0.6870(2)	0.7198(2)	0.2149(6)	22(1)^{b,c}
C16	0.6979	0.7371	0.0573	22(1)^{b,c}
C17	0.7408	0.7149	0.0053	22(1)^{b,c}
C18	0.7564	0.6840	0.1308	22(1)^{b,c}
C19	0.7232	0.6870	0.2604	22(1)^{b,c}
C15a	0.6840(2)	0.7309(2)	0.1595(6)	22(1)^{b,c}
C16a	0.7086	0.7358	0.0098	22(1)^{b,c}
C17a	0.7498	0.7065	0.0159	22(1)^{b,c}
C18a	0.7508	0.6836	0.1694	22(1)^{b,c}
C19a	0.7101	0.6987	0.2581	22(1)^{b,c}

[a] Equivalent isotropic U_{eq}, defined as one-third of the trace of the orthogonalized $\mathbf{U}_{ij}$ tensor; in 10^{-1} pm^2. [b] Atoms calculated as rigid groups have a standard deviation for the first atom only. [c] Disordered Cp ligands with a population of $^1/_2$ each.

The 2,5-dialkylated complexes **1c**,**d**,**f** form air-stable red crystals and are not air-sensitive, even in solution. In contrast to the unmethylated hydrides, they do not undergo H/D exchange with D_2O. With NaH no reaction takes place. Deprotonation of the sterically hindered tetramethyl complex **1d** can be effected by LiBu in THF, while the 2,5-dimethyl complex **1c** suffered reductive decomposition under these reaction conditions.

Crystal Structures of 1d and 1f. All attempts to grow crystals of **1a** suitable for X-ray diffraction work were unsuccessful. However, the chemically robust derivatives **1d**,**f** readily gave good crystals which allowed the determination of their structures at low temperature (**1d**, Figure 1, Tables 1 and 2; **1f**, Figure 2, Tables 3 and 4). In the case of **1d** rotational disorder of the cyclopentadienyl ring was encountered in spite of the low temperature of the measurement.

The molecules of **1d**,**f** show a bent-sandwich structure with bending angles[15] of 165.2 and 164.3°, respectively. Both structures deviate very little from lateral symmetry, except for the rotational orientation of the phenyl group.

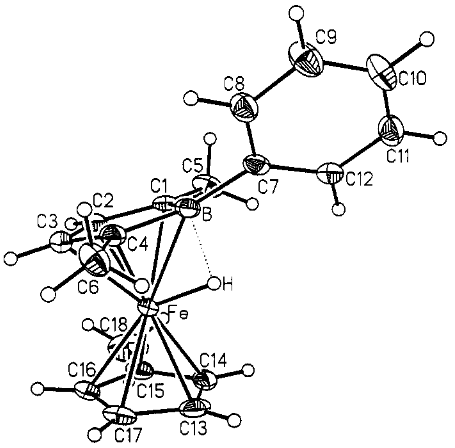

Figure 2. Presentation of the molecular structure (50% ellipsoids) of $(C_5H_4Me)FeH(2,5\text{-}Me_2C_4H_2BPh)$ (**1f**).

Table 2. Selected Bond Distances and Bond Angles for 1d

	(a) Bond Distances (pm)		
	Metal–Ligand and Borole		
Fe–B	215.1(4)	Fe–C1	209.3(3)
Fe–H	147(3)	Fe–C2	206.7(3)
B–H	151(3)	Fe–C3	208.1(3)
		Fe–C4	210.3(3)
B–C1	156.5(5)	B–C9	160.8(4)
C1–C2	141.4(5)	C1–C5	149.9(5)
C2–C3	143.7(5)	C2–C6	150.8(5)
C3–C4	142.7(4)	C3–C7	149.6(5)
B–C4	156.2(5)	C4–C8	149.9(5)
	Cp Ring C15···C19a		
Fe–C_{min}	203.9(5)	Fe–C_{av}	206.8
Fe–C_{max}	209.4(5)		
	(b) Bond Angles (deg)		
Fe–H–B	92(2)	B–C1–C2	108.7(3)
C1–B–C4	101.8(3)	C1–C2–C3	110.7(3)
C1–B–C9	127.3(3)	C2–C3–C4	110.0(3)
C4–B–C9	128.5(3)	C3–C4–B	108.7(3)

Table 3. Coordinates of Non-Hydrogen Atoms and of the Hydridic Hydrogen Atom for 1f

atom	*x*	*y*	*z*	$U_{eq}{}^a$
Fe	0.5989(1)	0.2173(1)	0.8376(1)	16(1)
H	0.4962(20)	0.3161(30)	0.8041(15)	35(6)
B	0.5606(1)	0.4356(2)	0.7655(1)	19(1)
C1	0.6573(2)	0.4528(2)	0.8518(1)	20(1)
C2	0.7479(2)	0.3878(2)	0.8453(1)	21(1)
C3	0.7218(2)	0.2606(2)	0.7652(1)	22(1)
C4	0.6129(2)	0.3054(2)	0.7151(1)	21(1)
C5	0.6578(2)	0.5536(2)	0.9305(1)	29(1)
C6	0.5598(2)	0.2265(2)	0.6308(1)	29(1)
C7	0.4654(2)	0.5641(2)	0.7277(1)	19(1)
C8	0.4670(2)	0.6333(2)	0.6471(1)	25(1)
C9	0.3915(2)	0.7533(3)	0.6132(1)	33(1)
C10	0.3099(2)	0.8074(3)	0.6580(1)	32(1)
C11	0.3057(2)	0.7419(3)	0.7376(1)	28(1)
C12	0.3827(2)	0.6224(2)	0.7717(1)	22(1)
C13	0.4726(2)	0.0607(2)	0.8561(1)	30(1)
C14	0.5253(2)	0.1349(2)	0.9359(1)	28(1)
C15	0.6448(2)	0.0963(2)	0.9539(1)	25(1)
C16	0.6644(2)	0.0002(2)	0.8848(1)	25(1)
C17	0.5575(2)	−0.0233(2)	0.8248(1)	29(1)
C18	0.7331(2)	0.1416(3)	1.0327(2)	45(1)

[a] Equivalent isotropic U_{eq}, defined as one-third of the trace of the orthogonalized $\mathbf{U}_{ij}$ tensor; in 10^{-1} pm^2.

---

(15) The bending angle is the angle spanned by the perpendiculars of the two rings.

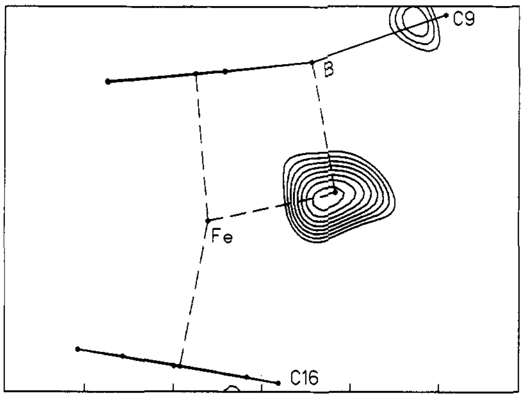

Figure 3. Difference-electron density map for the hydrogen atom of **1d** presented with isoelectron lines (outer line 0.30 × 10^{-6} e/pm^3, steps in 0.05 × 10^{-6} e/pm^3).

Table 4. Selected Bond Distances and Bond Angles for 1f

	(a) Bond Distances (pm)		
	Metal–Ligand and Borole		
Fe–B	215.5(2)	Fe–C1	210.1(2)
Fe–H	147.5(23)	Fe–C2	205.8(2)
B–H	146.1(26)	Fe–C3	206.0(2)
		Fe–C4	211.0(2)
B–C1	157.8(2)	B–C7	159.0(3)
C1–C2	141.0(3)	C1–C5	150.4(3)
C2–C3	143.9(3)	C4–C6	150.2(3)
C3–C4	141.2(3)		
B–C4	156.7(3)		
	Cp Ring C13···C17		
Fe–C_{min}	205.1(2)	C–C_{min}	139.5(3)
Fe–C_{max}	208.1(2)	C–C_{max}	142.6(3)
Fe–C_{av}	206.6	C–C_{av}	141.5
	(b) Bond Angles (deg)		
Fe–H–B	94.5(14)	B–C1–C2	107.7(2)
C1–B–C4	102.3(1)	C1–C2–C3	111.1(2)
C1–B–C7	126.3(2)	C2–C3–C4	110.8(2)
C4–B–C7	127.1(2)	C3–C4–B	108.1(2)

The C–C bond lengths within the borole ring (141.4/143.7/142.7 pm for **1d** and 141.0/143.9/141.2 pm for **1f**) show that metal-to-ligand back-bonding into the diene region of the borole ring is less important than in Fe$(CO)_3(C_4H_4BPh)$ (**3a**) (142.6/141.7/143.5 pm).[13] This is not unexpected for d^6 systems, where back-bonding is generally less favorable than in d^8 systems.[16] On the other hand, the Fe–B distance (215.1(4) pm for **1d** and 215.5(2) pm for **1f**) is much shorter than for **3a** (228.6(2) pm).[13]

The most interesting feature of the structure is the position of the hydridic hydrogen atom. The Fe–H distance (147(3) pm for **1d** and 147.5(23) pm for **1f**) is similar to Fe–H distances found in classical iron hydride complexes such as *cis,mer*-$FeH_2(H_2)(PEtPh_2)_3$ (151.4(6) and 153.8(7) pm, determined by neutron diffraction at 27 K).[17] The B–H distance (151(3) pm for **1d** and 146.1(26) pm for **1f**) is rather long for a three-center Fe–H–B bond (cf., e.g., $Fe_2(B_3H_7)(CO)_6$ with B–H = 127(4) and 137(4) pm and Fe–H = 156(4) and 166(4) pm for Fe–H–B, determined by X-ray diffraction[18]) and therefore does not represent unambiguous evidence for three-center bonding. However, there are several details which warrant the presence of a B–H bonding interaction. A cross section through the approximate mirror plane of the sandwich moiety of **1d** (Figure 3) shows a pronounced bending of the hydrogen atom toward the boron atom. The slip distortion[19] of the iron toward the diene region of the borole ring (2.1 pm for **1d** and 3.6 pm for **1f**) is unusually small (cf. 6.9 pm for **3a**[13]), thus holding the iron atom closer to the boron atom. The usual folding of the borole ring along the line C1,C4 and away from the metal is reduced and amounts to only 0.8 and 0.5° (cf. 6.1° for **3a**[13]). In addition, the sum of the bonding angles at the boron atom is slightly but significantly smaller than 360° (357.6° for **1d** and 355.7° for **1f**), with the phenyl group bending away from the hydridic hydrogen.

It could be argued that a disordered racemate of agostic enantiomers **1-A** would produce apparent lateral symmetry. However, a careful check of the difference Fourier synthesis for **1d** that gave the position of the hydridic hydrogen did not show a significant elongation of the corresponding electron density in the direction perpendicular to the molecular mirror plane. Hence, we conclude the following: all evidence from two very similar structure determinations shows that the hydrides of type **1** possess the laterally symmetric ground state **1-G** (≡**1**), which involves an Fe–H–B three-center interaction with weak B–H bonding.

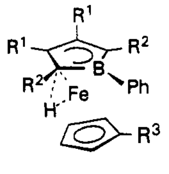

1-A

Spectroscopic Characterization. The hydrides **1a,b,e**, without substituents at the 2,5-position, show temperature-dependent ^1H and ^{11}B NMR spectra which indicate the presence of two dynamic processes. At room temperature the ^1H NMR (80-MHz) spectrum for **1a** displays broadened signals for the 2,5-protons of the borole ring and the hydridic proton; fine structure due to the coupling between the borole protons cannot be discerned. When the temperature is raised, the signals of the 2,5-protons and of the hydridic proton coalesce at 333 K. Then a single signal emerges for these three protons which sharpens upon further heating up to the limit of beginning decomposition at 383 K. On the other hand, when the temperature is lowered, the signal of the hydridic proton sharpens and the expected pattern for an AA′BB′ spin system with its characteristic fine structure[8] appears for the borole protons. There is no appreciable direct ^{11}B–^1H coupling, as the line width of the hydridic hydrogen is rather small (e.g. for **1a**, 4 Hz at 243 K and 7 Hz at 193 K); in fact, this observation is not unexpected, as the B–H interaction will be mediated essentially by the $2p_z$ orbital of the boron with little admixture of s character at boron. The exchange of the 2,5-protons and the hydridic proton is an intramolecular process, as it is independent of the concentration of **1a**. Simulation of the dynamic NMR spectra establishes a free energy of activation ΔG^{*}_{333} = 17.0 ± 0.7 kcal/mol for **1a** and 16.7 ± 0.7 kcal/mol for **1b**.[20]

---

[16] Elian, M.; Hoffmann, R. *Inorg. Chem.* **1975**, *14*, 1058.

[17] Van Der Sluys, L. S.; Eckert, J.; Eisenstein, O.; Hall, J. H.; Huffman, J. C.; Jackson, S. A.; Koetzle, T. F.; Kubas, G. J.; Vergamini, P. J.; Caulton, K. G. *J. Am. Chem. Soc.* **1990**, *112*, 4831.

[18] Haller, K. J.; Andersen, E. L.; Fehlner, T. P. *Inorg. Chem.* **1981**, *20*, 309.

[19] The slip distortion is the distance between the geometric center of the heterocycle and the projection of the metal atom.

[20] The simulation was carried out with the program GEM-NMR by C. G. Kreiter and U. Seimet, University of Kaiserslautern.

Scheme 3

1a-G **1a-A**

Table 5. Selected $\delta(^{11}\mathrm{B})$ Data for the Hydrides 1a-f

compd	T (K)	$\delta(^{11}\mathrm{B})$	compd	T (K)	$\delta(^{11}\mathrm{B})$
1a	203	-6.0	**1c**	299	-8.6
	299	-3.5	**1d**	299	-8.7
	363	1.5	**1e**	299	-5.5
1b	213	-7.3	**1f**	299	-8.0
	323	-5.7			
	383	-1.9			

Furthermore, the protons of **1a,b,e** that are not involved in the exchange process show a marked temperature dependence of their chemical shifts down to the practical low-temperature limit of 193 K (e.g. for **1a** $\delta(^1\mathrm{H})$ 7.60 ($\mathrm{H_o}$) and 4.03 (Cp) at 383 K versus $\delta(^1\mathrm{H})$ 7.99 ($\mathrm{H_o}$) and 3.66 (Cp) at 193 K). The $^{11}\mathrm{B}$ NMR signal occurs at a very high field compared to that for non-hydridic borole sandwich complexes[2] (e.g. for $\mathrm{CpCo(C_4H_4BPh)}$ $\delta(^{11}\mathrm{B})$ 18.0[8]) and, in addition, shows a significant shift to higher field at lower temperatures. In contrast to these observations, the spectra of dimethylated hydrides **1c,d** show no significant temperature dependence and their $\delta(^{11}\mathrm{B})$ shifts are comparable to the shifts of **1a,b** at the lowest temperature. Some pertinent data are collected in Table 5.

These data indicate a fast equilibrium between at least two species for **1a,b,e**, with a ground-state species of type **1-G** (Scheme 3). As the higher energy isomer we propose the agostic species **1-A** with a much less shielded boron atom. The closely related $\mathrm{MnH(CO)_3(C_4H_4BPh)}$ with $\delta(^{11}\mathrm{B})$ 31.9 possesses an agostic ground-state structure, as found by low-temperature NMR.[21] Related classical structures with boracyclopentenyl ligands also show deshielded boron, e.g. for $\mathrm{CpNi(C_4H_5BPh)}$ $\delta(^{11}\mathrm{B})$ 35[22] and for $\mathrm{Co(CO)_2(PMe_3)(C_4H_5BPh)}$ $\delta(^{11}\mathrm{B})$ 30.0.[1] If we assume $\delta(^{11}\mathrm{B})$ −7.0 for **1a-G** (cf. Table 5) and $\delta(^{11}\mathrm{B})$ 32 for **1a-A**, the boron shift of $\delta(^{11}\mathrm{B})$ −3.4 at 299 K gives a rough estimate of 9% for the share of **1a-A** in a solution of **1a** at 299 K corresponding to ΔG = 1.4 kcal/mol.

Within the framework of Scheme 3 the two enantiomers of **1a-A** are in rapid equilibrium via **1a-G**, that is, by a path for the proton on the endo side of the borole ring. It should be noted that this low-energy process conserves the identity of the hydridic proton. A migration of the proton 5exo-H to C-2 across the exo face of the borole ligand also interconverts the two enantiomers of **1a-A** but, in addition, exchanges the 2,5-borole protons and the hydridic proton. It seems likely that this migration across the exo face is the mechanism of the above-described intramolecular exchange process. To gain further support for the existence of agostic isomers of type **1-A** and for the mechanisms just postulated, it seemed desirable to look at the bonding situation in the hydrides **1** more closely.

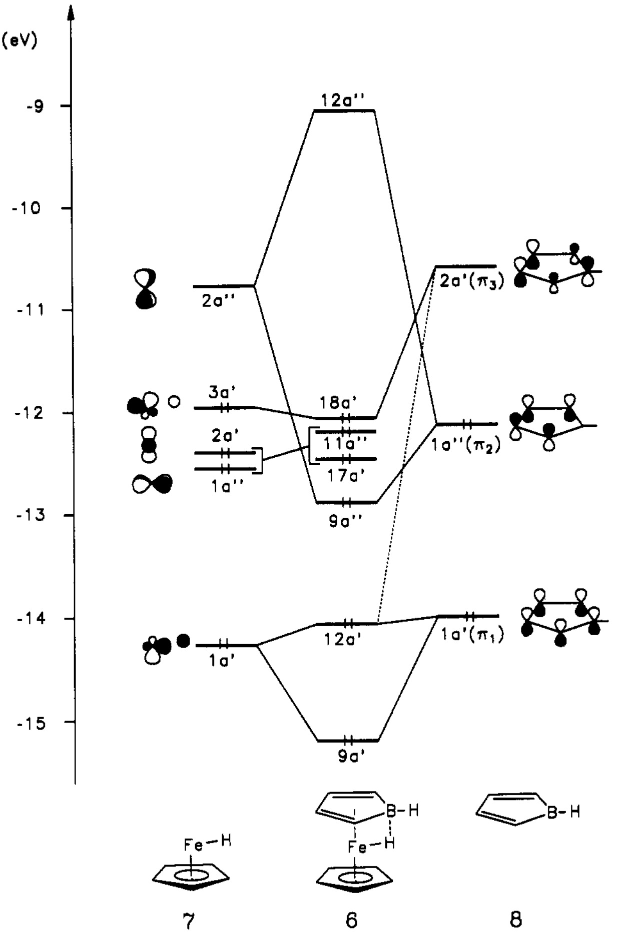

Figure 4. Frontier orbital diagram for $\mathrm{CpFeH(C_4H_4BH)}$ (**6**).

Electronic Ground-State Structure of CpFeH-($\mathrm{C_4H_4BH}$). Using Hoffmann's fragment-MO approach, we derive the frontier MO's of $\mathrm{CpFeH(C_4H_4BH)}$ (**6**) from the CpFeH (**7**) fragment and the borole ligand $\mathrm{C_4H_4BH}$ (**8**). The most important orbitals of **7** are shown on the left side of Figure 4. Going from lower to higher energy, one finds the 1a′ level, which is mainly composed of the 1s orbital of the hydrogen atom and the iron $d_{z^2-y^2}$ orbital. In the localized picture it describes the Fe–H σ bond. The 1a′ fragment MO is followed by the three metal-centered MO's 1a″, 2a′, and 3a′. The last two can be described as linear combinations of the d_{z^2}, $d_{x^2-y^2}$, and d_{yz} iron orbitals, while 1a″ is the d_{xy} orbital. The low-lying LUMO, 2a″, is the d_{xz} orbital of the iron center.

Fragment **8** contributes two occupied π MO's (1a′(π_1) and 1a″(π_2)) together with a low-lying empty MO (2a′(π_3)) (see Figure 4, right). For the sake of clarity we omitted the σ MO's of **8** as well as all MO's localized on the Cp ring of **7** in Figure 4.

The frontier MO's of **6** arise from the interaction of both fragments, as shown in the center part of Figure 4. For their construction we make use of the noncrossing rule. The most important stabilizing contributions are achieved by the interactions of the HOMO and LUMO of both fragments. The interaction of the occupied 1a″(π_2) of **8** with the empty 2a″ of **7** gives rise to the bonding level 9a″ and the LUMO 12a″ of **6**. The HOMO of **7** (3a′) interacts with π_3 of **8**, yielding 18a′ (HOMO) and 19a′ (not shown in Figure 4) of **6**. This interaction leads to a charge transfer from the iron to the borole ligand. This can best be seen from the net charges of the iron in **7** (q(Fe) = −0.44) and **6** (q(Fe) = +0.10). This change is due to metal-to-ligand back-bonding and to some extent to the three-center Fe–H–B interaction in **6**. The orbital 1a′ of **7** (Fe–H

---

[21] The low-temperature limiting $^{13}\mathrm{C}$ NMR spectrum of $\mathrm{MnH(CO)_3(C_4H_4BPh)}$ shows four different ring carbon atoms with a doublet of doublets for C-5 (^1J = 161 ± 5 and 92 ± 5 Hz): Herberich, G. E.; Köffer, D. P. J.; Kreiter, C. G., unpublished results.

[22] Herberich, G. E.; Hausmann, I.; Hessner, B.; Negele, M. *J. Organomet. Chem.* **1989**, *362*, 259.

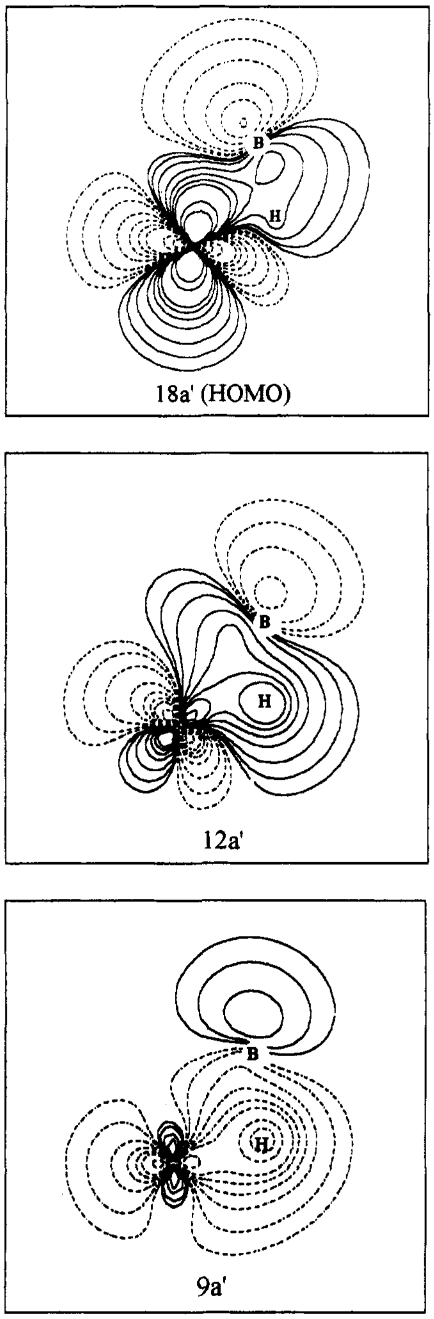

18a' (HOMO)

12a'

9a'

Figure 5. Contour plots of the orbitals 18a′, 12a′, and 9a′ in the *yz* plane.

σ bond) interacts with 1a′(π_1) and 2a′(π_3) of **8**, yielding 9a′ and 12a′ of **6**. The interaction with the unoccupied 2a′(π_3) level allows an electron density transfer from the Fe–H σ bond to the borole ligand and describes the Fe–H–B bond. The contour plots of 18a′, 12a′, and 9a′ are shown in Figure 5. In all three cases a mixing between 3d orbitals at the iron, the 1s orbital at the hydrogen, and the 2p orbital at the boron center can be seen.

Search for Tautomeric Structures and Dynamic Processes. In Figure 6 we have shown the total energy of **6** as a function of an angle α which describes the rotation of the hydrogen around the *z* axis starting from the *yz* plane (α = 0°). Energy values are calculated by using the extended Hückel method, changing only α and leaving all other parameters constant.

Due to the rotation of the hydrogen the stabilizing Fe–H–B interaction vanishes. At α = 140° we obtain the local minimum **6-C**. This local minimum is due to an interaction between the hydrogen at the iron and the p_z AO at C-3. The energy difference between the global minimum **6-G** and **6-C** is predicted to be 36 kcal/mol. The activation energy for the reaction of **6-A** to give **6-C** is calculated to be 40 kcal/mol.

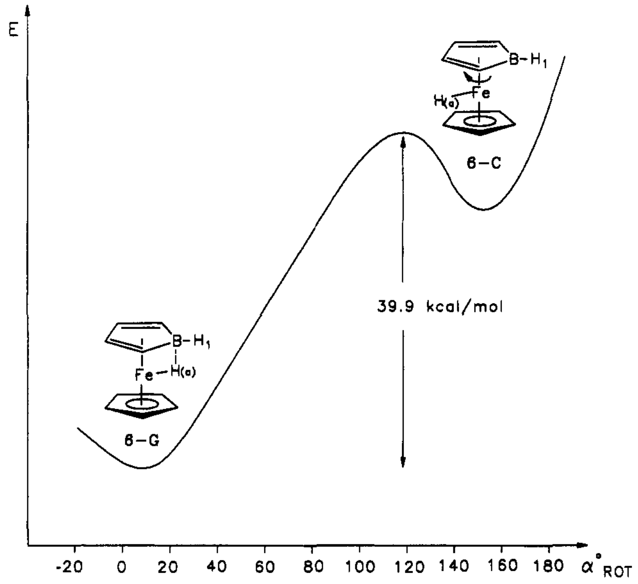

Figure 6. Total energy of **6** as a function of the rotational angle α (see text).

Table 6. Cyclic Voltammetry Data[a]

complex	couple	E (V)[b]	ΔE (mV)[c]	i_c/i_a	v (V/s)	solvent
1a	+/0	0.72	*d*		0.1	DME
1a–A	0/–	–0.76	*d*		0.05–1.0	
1a–G	0/–	–2.03	*d*		0.05–1.0	
1d	+/0	0.68	*d*		0.1	DME
	0/–	–2.30	70	0.97	0.02–0.5	
5a$^-$	0/–	–0.79	75	1.0	0.05–5	DME
	–/2–	–2.25	*d*		0.1	DME

[a] Data reported for platinum working electrode at room temperature; electrolyte concentration is 0.1 M. [b] Potentials are vs SCE; $E°$ reported for reversible systems, peak potentials ($E_p{}^c$, $E_p{}^a$) for irreversible processes. [c] Peak separation, exceeds 60–70 mV for reversible signals in DME due to uncompensated *iR* drop. [d] Irreversible.

To rationalize the intramolecular proton exchange of **1a,b,e**, we have carried out model calculations on **6**. Since a rigorous treatment is not possible because of the shortcomings of the extended Hückel method with respect to the optimization of bond lengths, we changed only a few parameters. First, we move the hydrogen at C-2 of the borole ring, H2, away from the borole plane and we rotate the Fe–H bond by 70° out of the *yz* plane (points 1–6 in Figure 7). The energy can be reduced by moving the hydrogen at the iron atom (H(a)) to C-2 (points 7 and 10). The bending of H2 reduces the activation energy from 40 kcal/mol (Figure 6) to 27 kcal/mol (Figure 7). The calculated energy difference between **6-G** and the agostic isomer **6-A** amounts to 15 kcal/mol. In the following steps (11–16) we move H(a), H2, and H1 in such a way that at the end the boratacyclopentadiene species **6-B** is obtained. For this movement an activation energy of 9.2 kcal/mol is estimated. The second intermediate **6-B** is predicted at the same energy as **6-A**. The migration of H2 to C-5 is analogous to the previous step (**6-A** to **6-B**), and the migration of H5 to Fe is identical with the first step. If, however, H2 in **6-A** is moved directly to C-5 without the detour via **6-B**, an additional energy barrier of 33 kcal/mol is calculated. Hence, this "direct path" seems very unlikely.

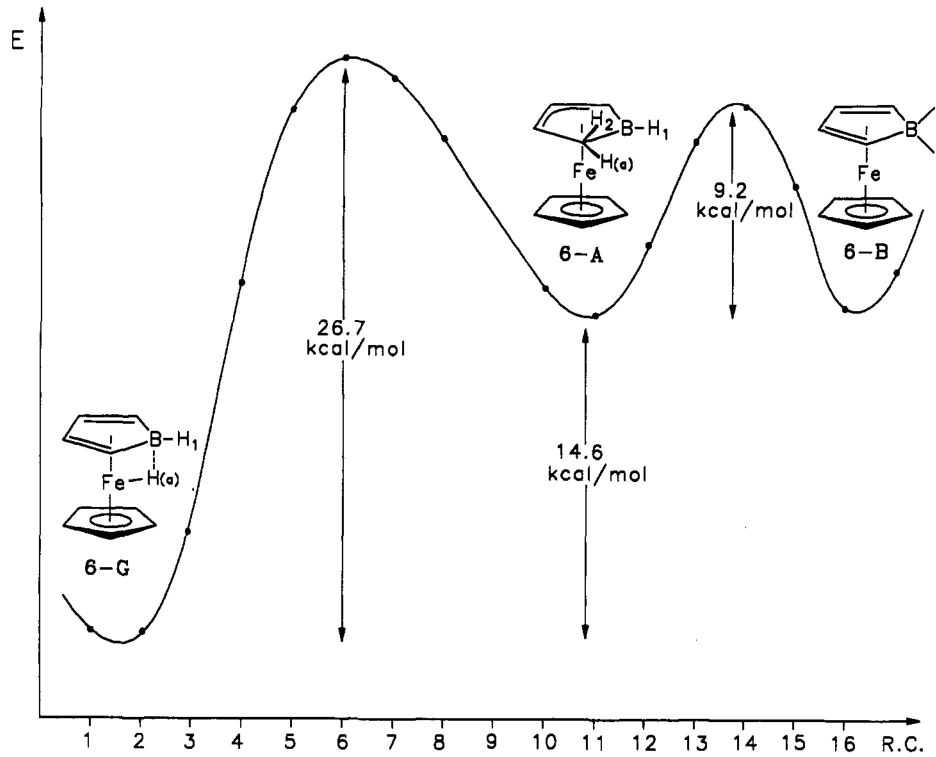

Figure 7. Total energy of **6** as a function of the reaction coordinate for hydrogen migration (see text).

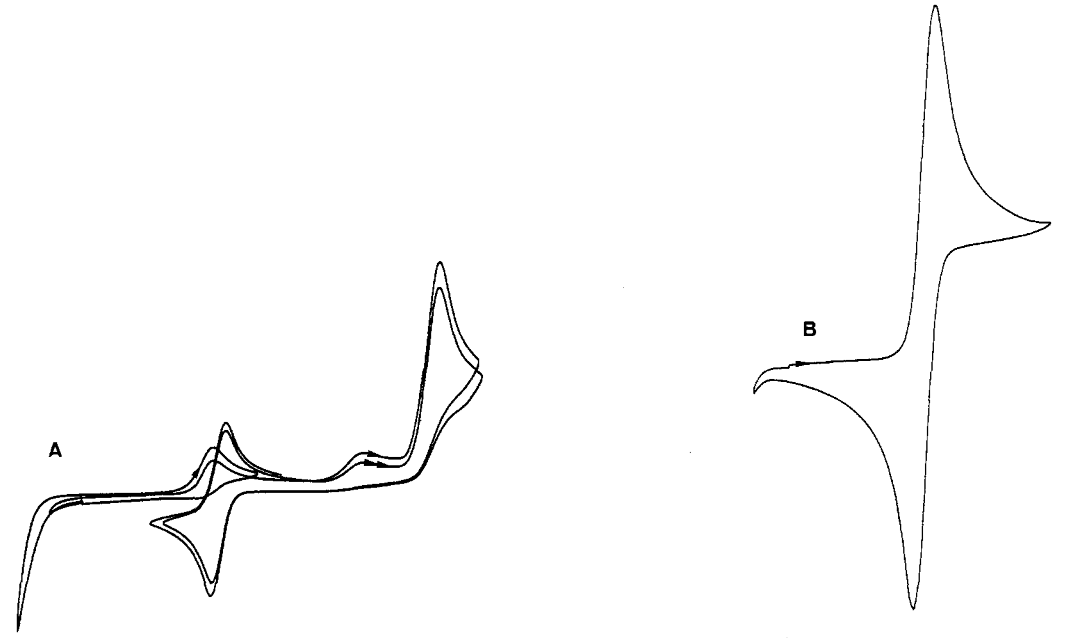

Figure 8. Cyclic voltammograms for **1a** (A) and for **5a**/**5a**$^-$ (B).

We also considered the tautomer (CpH)Fe(C_4H_4BH) (**6-D**) with the agostic interaction Fe–H–C(Cp). For this agostic isomer the calculated energy difference between **6-D** and **6-G** amounts to 25 kcal/mol, while the energy difference between **6-A** and **6-G** is predicted to be 15 kcal/mol.

Electrochemical Results and Identification of the 17e Complex CpFe(C_4H_4BPh) (5a) by EPR and Paramagnetic NMR Spectroscopy. Investigation of **1a** by cyclic voltammetry showed a complex behavior (Figure 8, Table 6). On reducing **1a** in Bu_4NPF_6/DME solution at room temperature, we observed two irreversible reduction peaks at −0.76 and −2.03 V. The reduction peak at −0.76 V exhibits reoxidation at −58 °C (v = 0.2 V/s), with i_a/i_c being 0.97. Both reductions yield the same product represented by the reversible oxidation wave at $E°$ = −0.79 V. The cyclic voltammogram of Na-**5a** shows a reversible oxidation wave at the same potential. These observations suggest that the irreversible reduction of **1a** results in the formation of anion **5a**$^-$, via hydrogen abstraction from the short-lived intermediate **1a**$^-$, and that **5a**$^-$ shows a reversible oxidation to the paramagnetic species **5a** (Scheme 4).

The anion **5a**$^-$ is very air-sensitive and undergoes fast oxidation with oxygen even at low temperature. Dilute solutions of **5a** in THF can readily be generated, e.g. from [Li(TMEDA)]**5a** in THF by controlled oxidation with air

Scheme 4

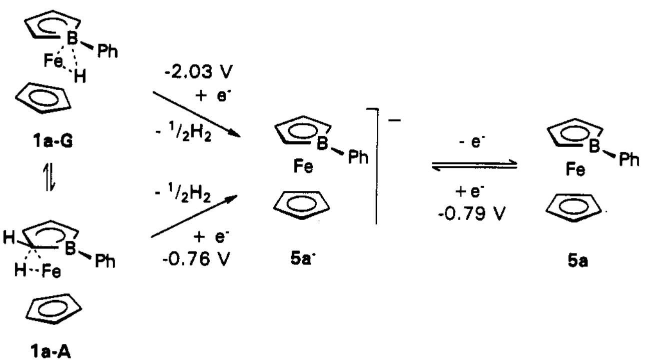

(cf. NMR experiments below), and reduction with potassium regenerates **5a**$^-$. However, attempts to isolate **5a** have failed so far. Frozen solutions of **5a** display an EPR spectrum (100 K, glassy frozen THF-d_8, $g_\parallel$ = 3.05 and $g_\perp$ = 1.97).

The observation of two irreversible reduction processes is in agreement with the hypothesis of an equilibrium between the two isomers **1a-G** and **1a-A**. The first peak at −0.76 V is assigned to the reduction of **1a-A** and the peak at −2.03 V to that of **1a-G**. Bulk electrolysis of **1a** at −1.0 V effected complete conversion to **5a**$^-$; in a subsequent cyclic voltammogram the reduction peak at −2.03 V had also disappeared. In striking contrast to **1a** the 2,3,4,5-tetramethyl derivative **1d** shows a single reversible reduction at −2.30 V. This process corresponds to the reduction of **1a-G**; the four additional methyl groups of **1d** effect a cathodic shift of the reduction and a stabilization of the reduced species **1d**$^-$ in agreement with general trends.[23]

By stepwise oxidation of ^{1}H NMR samples of [Li(TMEDA)]**5a**[9] in THF-d_8 with air an increasing shift of most signals is observed which is caused by the paramagnetism of **5a**. This process comes to an end when the formation of **5a** is completed and can be reversed by reduction of **5a** at a potassium mirror in the sample tube (Figure 9, Table 7). The anion **5a**$^-$ is stable for weeks in contact with metallic potassium.

The observation of only one signal for every set of equivalent protons in diamagnetic **5a**$^-$, paramagnetic **5a**, and mixtures of both species indicates a rapid symmetrical electron transfer between these two species. Thus, the observed chemical shift δ_{obs} for mixtures of **5a**/**5a**$^-$ is the mean of the chemical shifts δ_{dia} and δ_{para} weighted with the mole fractions f_d and f_p of diamagnetic **5a**$^-$ and paramagnetic **5a**, respectively (eq 1). Hence, δ_{obs} is linearly

$$\delta_{obs} = f_d\delta_{dia} + f_p\delta_{para} \qquad (1)$$

$$\delta_p = \delta_{para} - \delta_{dia} \qquad (2)$$

dependent on the paramagnetic mole fraction f_p. This relationship allows an unambiguous correlation between the spectra of both redox states, and in this way the paramagnetic spectra of **5a** can be assigned easily (Table 8).[24] The difference $\delta_{para} - \delta_{dia}$ represents the paramagnetic shift δ_p (eq 2).

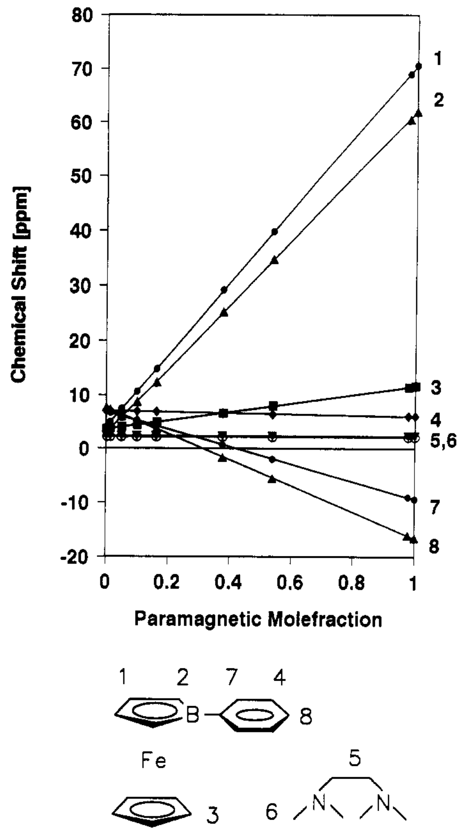

Figure 9. Chemical shifts δ_{obs} for **5a**/**5a**$^-$ as a function of paramagnetic mole fraction f_p.

Table 7. Chemical Shifts δ_{obs} (ppm) for ^{1}H NMR Signals as a Function of the Paramagnetic Mole Fraction f_p

	signal[a]							
f_p	1	2	3	4	5	6	7	8
0.000	4.03	2.82	3.61	7.05	2.30	2.15	6.92	7.65
0.013	4.93	3.70	3.73	7.03	2.30	2.15	6.65	7.27
0.050	7.45	5.95	3.98	7.00	2.30	2.15	6.04	6.35
0.100	10.65	8.70	4.37	6.95	2.30	2.15	5.24	5.24
0.162	14.80	12.42	4.87	6.88	2.30	2.15	4.21	3.60
0.377	29.2	25.3	6.6	6.60	2.30	2.15	0.65	-1.70
0.538	39.8	34.8	8.0	6.43	2.30	2.15	-1.98	-5.60
0.978	69.0	60.5	11.5	6.08	2.30	2.15	-9.0	-16.0
1.000	70.6	62.0	11.7	6.06	2.30	2.15	-9.4	-16.5

[a] For signal designation see Figure 9.

Table 8. Paramagnetic Shifts (ppm) and Line Widths (Hz) for ^{1}H NMR Signals of 5a

	signal[a]							
	1	2	3	4	5	6	7	8
δ_p[b]	66.6	59.2	8.1	1.0	0	0	−16.3	−24.2
LW$_p$[c]	680	470	290	0	0	0	20	46

[a] For signal designation see Figure 9. [b] See eq 2. [c] LW$_p$ = [line width (f_p = 1)] − [line width (f_p = 0)].

All protons of **5a** show the paramagnetic shift δ_p with respect to the diamagnetic line positions of **5a**$^-$ (Table 8), while the ligand TMEDA of the gegenion Li$^+$ remains unaffected. Within **5a** the paramagnetic shifts vary widely. The strong dispersion of line width for the paramagnetic NMR signals indicates that there is more than one cause for this situation.[25] This point is presently under study.

---

[23] (a) Koelle, U.; Khouzami, F. *Angew. Chem.* **1980**, *92*, 658; *Angew. Chem., Int. Ed. Engl.* **1980**, *19*, 640. (b) Richardson, D. E.; Ryan, M. F.; Khan, M. N. I.; Maxwell, K. A. *J. Am. Chem. Soc.* **1992**, *114*, 10482.

[24] (a) Köhler, F. H.; Zenneck, U.; Edwin, J.; Siebert, W. *J. Organomet. Chem.* **1981**, *208*, 137. (b) Zwecker, J.; Kuhlmann, T.; Pritzkow, H.; Siebert, W.; Zenneck, U. *Organometallics* **1988**, *7*, 2316. (c) Stephan, M.; Davis, J. H.; Meng, X.; Chase, K. J.; Hauss, J.; Zenneck, U.; Pritzkow, H.; Siebert, W.; Grimes, R. N. *J. Am. Chem. Soc.* **1992**, *114*, 5214.

Scheme 5

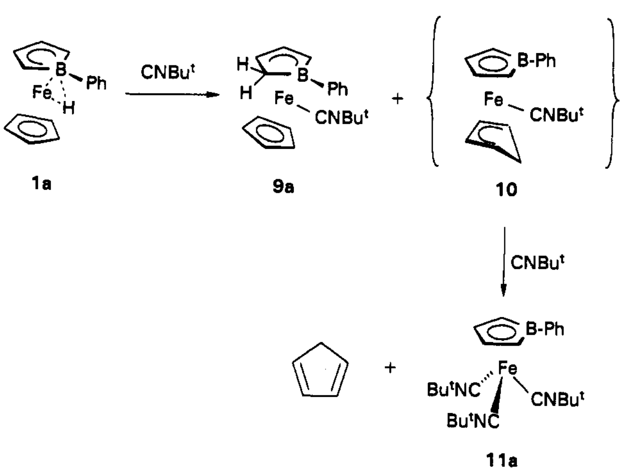

Reactivity of 1a. Chemical Evidence for the Existence of the Agostic Isomer 1a-A. Many agostic compounds add 2e donors such as CO or isocyanides with a concomitant shift of the agostic hydrogen atom.[26] We therefore investigated the reaction of **1a** with CNBu^t. When the reaction was monitored by NMR spectroscopy, three products were seen after a few hours at room temperature (Scheme 5). Treating **1a** with an approximately equimolar amount of CNBu^t (1.1 equiv) yielded a mixture of unconsumed **1a** (29%), the addition product CpFe(CNBu^t)(C_4H_5BPh) (**9a**; 53%), and Fe(CNBu^t)$_3$(C_4H_4BPh) (**11a**) together with free cyclopentadiene (each 18%). With an excess of CNBu^t **1a** was consumed completely. The products **9a** (51%) and **11a** (49%) did not react any further with unconsumed isocyanide. While **11a** is a robust compound which could readily be isolated, **9a** decomposed on attempted purification by chromatography. Our observations suggest two parallel reaction channels, one of these giving the observed product **9a** while the other one, via the hypothetical intermediate **10**, forms **11a** and cyclopentadiene.

We repeated the above experiment with deuterated **1a**. Treatment of the trideutero complex **1a**-d_3 (95% deuteration) with excess CNBu^t gave **9a**-d_3 (73%) and **11a**-d_2 and C_5H_5D (each 27%). The NMR spectra of the complex products showed the deuterium to be in the 2-/5-position of the C_4B ring ligands only. Cyclopentadiene was captured with maleic acid anhydride as the Diels–Alder adduct **12**. Examination of **12** by mass spectroscopy showed the presence of just one deuterium label (85%). Thus, there is essentially no isotopic scrambling.

Shining light onto the solution in presence of excess CNBu^t caused a slow conversion of **9a** to **11a**. Light-induced primary dissociation of **9a** is thought to give **1a** (via **1a-A**) and CNBu^t, which then can recombine to form **9a** and **11a** (via **10**) until all material is transformed into the final product **11a**.

Scheme 5 implies that the proposed intermediate **10** should readily react with CNBu^t to give **11a** and cyclopentadiene. Complex **10** could be prepared independently from Fe(CO)$_2$(CNBu^t)(C_4H_4BPh)[9] by irradiation in the presence of cyclopentadiene. When **10** was then treated with an excess of CNBu^t, very fast degradation took place to give **11a** and free cyclopentadiene (Scheme 6). Exposing a solution of the cyclopentadiene complex **10** in C_6D_6 to light induces disproportionation and produces **1a** (60%), **11a** (40%), and free cyclopentadiene (Scheme 6). Again the light-induced primary dissociation of **10** will give **1a** and CNBu^t followed by thermal degradation of more cyclopentadiene complex **10** by the liberated CNBu^t.

Scheme 6

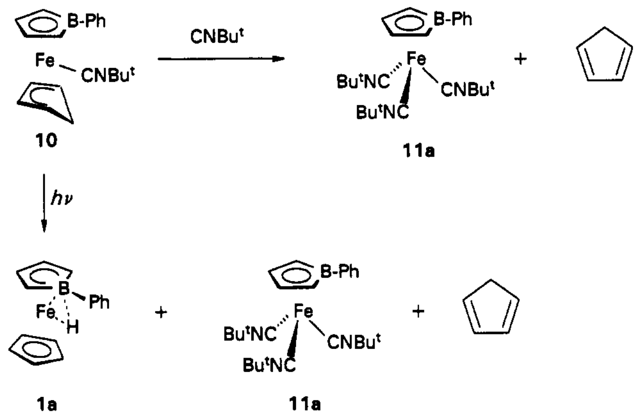

The 2,5-dimethyl derivative **1c** reacts with CNBu^t in the same way as **1a**, albeit at a much lower rate. While the reaction of **1a** took a few hours at room temperature, the reaction of **1c** required 30 days and afforded the η^4-boracyclopentenyl complex **9c** (25%) and the tris(isocyanide) complex **11c** (75%).

Discussion

(Borole)(cyclopentadienyl)iron hydrides **1** are a new family of complex iron hydrides. The laterally symmetric ground-state structure **1-G** of the 2,5-dialkylated members (**1c,d,f–h**) is unambiguously established by our X-ray structural work. While the B–H distances are rather long for Fe–H–B three-center bonding, several structural details provide evidence for the presence of a presumably weak Fe–H–B three-center interaction; this interpretation is strengthened by the analysis of the bonding situation on the basis of extended Hückel calculations. For the 2,5-unsubstituted derivatives (**1a,b,e**) tautomeric structures (the ones of type **1-A**) are very close in energy. Comparison of the low-temperature NMR data shows, however, that these derivatives possess the same type of ground-state structure **1-G**.

The temperature dependence of the chemical shift data for the 2,5-unsubstituted derivatives required the assumption of an equilibrium between at least two tautomers. The choice of agostic isomers of type **1-A** as higher energy tautomers cannot be stringently deduced from the NMR spectra but merely relies on good agreement with our spectral observations and on general chemical intuition.

At this point our extended Hückel calculations were used to find energy minima for the location of the hydrogen atom during its rotation around the axis of the borataferrocene sandwich and the migration across the exo face of the borole ligand. Three important minima were found, one (**6-G**) for the ground state, one (**6-A**) corresponding to an agostic structure of type **1-A**, and a second one (**6-B**) corresponding to the structure of a borata-2,4-cyclopentadiene complex. We note here that a related complex with a 1-methyl-1-phenylborata-2,4-cyclopentadiene ligand, Li[Fe(CO)$_3$(C_4H_4BMePh)], has recently been observed experimentally as a low-temperature (<−50 °C) solution

---

(25) Keller, H. J. In *NMR Basic Principles and Progess*; Diehl, P., Fluck, E., Kosfeld, R., Eds.; Springer-Verlag: Berlin, 1970; Vol. 2, p 53.

(26) (a) Ittel, S. D.; Van-Catledge, F. A.; Jesson, J. P. *J. Am. Chem. Soc.* **1979**, *101*, 6905. (b) Lamanna, W.; Brookhart, M. *J. Am. Chem. Soc.* **1981**, *103*, 989.

species.[11] The calculations therefore support our interpretation of the NMR spectra of the hydrides **1**.

Two further minima, **1-C** and **1-D**, were found which lie at rather high energies and therefore are of little importance. In case of isomer **1-D** it is also experimentally clear from the ^{1}H NMR spectra that this isomer does not contribute to the tautomeric equilibrium of **1a**, as the Cp signal of **1a** does not show any line broadening.

Finally, in the reaction of **1a** and **1c** with CNBu^t the hydridic hydrogen is shifted to C2 of the borole ligand or alternatively to a Cp carbon atom (Scheme 5). This process is intramolecular, as no isotopic scrambling is observed. The addition of a 2e donor is a characteristic reaction of many agostic compounds.[26] In this vein we assume that the agostic isomers **1-A** and **1-D** respectively act as intermediates in the isonitrile addition reaction.

Experimental Section

General Procedures. Reactions were carried out under an atmosphere of dinitrogen by means of conventional Schlenk techniques. Pentane and hexane were distilled from Na/K alloy, toluene and ethereal solvents were distilled from sodium benzophenone ketyl, and methylene chloride was distilled from CaH_2. Alumina for chromatography (Woelm) was heated under a high vacuum at 300 °C and deactivated (7% H_2O, deoxygenated) after cooling. Melting points were measured in sealed capillaries and are uncorrected. Elemental analyses were performed by Analytische Laboratorien, D-51753 Engelskirchen, FRG.

NMR spectra were recorded on a Bruker WH 270 PFT spectrometer (^{1}H, 270 MHz; ^{13}C, 67.88 MHz), a Bruker WP 80 PFT spectrometer (^{1}H, 80 MHz), and a JEOL NM-PS-100 spectrometer (^{11}B, 32.08 MHz). The digital resolution was <0.5 Hz/point for ^{1}H and <1.0 Hz/point for ^{13}C spectra; half-widths of broad signals are given in parentheses. EPR spectra were recorded on a Bruker ESP 300 E spectrometer. DPPH (g = 2.0036) was used as a standard for determination of the g value. The paramagnetic NMR spectra were measured on a JEOL JNM GX 270 spectrometer. Infrared spectra were recorded on a Perkin-Elmer 842 spectrometer.

Preparation of 3b. A solution of 5.4 g (31.8 mmol) of 3,4-dimethyl-1-phenyl-3-borolene[12] (**2b**) and 2.1 mL (15.9 mmol) of $Fe(CO)_5$ in 150 mL of THF was irradiated for 7 days. The color of the solution changed from yellow to dark red. The reaction was monitored by IR spectroscopy. At the end of the reaction the solution was refluxed for 1 h. The solution was concentrated to 50 mL; then the same volume of alumina was added, and all volatiles were removed. The red, dry, solid material was transferred to a short column (4 cm wide) already charged with alumina to a height of 10 cm. The product was eluted with 500 mL of pentane. Crystallization of the product from 100 mL of pentane at −30 °C gave **3b** (2.25 g, 46%).

3b: yellow, almost air-stable needles; mp 101 °C; dec pt ca. 300 °C; MS m/z (I_{rel}) 308 (50, M^+), 224 (100, $M^+ - 3$ CO); IR (hexane, cm^{-1}) 2060 s (CO), 2002 s (CO), 1990 s (CO); ^{1}H NMR ($CDCl_3$) δ 7.60 (m, 2 H_o), 7.28 (m, 2 $H_m + H_p$), borole 3.63 (s, 2-/5-H) and 2.12 (s, 3-/4-Me); ^{11}B NMR ($CDCl_3$) δ 19.1; ^{13}C NMR ($CDCl_3$) δ 211.2 (s, 3 CO), 134.9 (d, ^1J = 155 Hz, 2 C_o), 128.6 (d, ^1J = 159 Hz, C_p), 127.8 (d, ^1J = 157 Hz, 2 C_m), borole 112.4 (s, C-3/-4), 77 (d br, C-2/-5, partly hidden by $CDCl_3$ signal), and 15.1 (q, ^1J = 128 Hz, 2-/5-Me). Anal. Calcd for $C_{15}H_{13}BFeO_3$: C, 58.51; H, 4.26. Found: C, 58.46; H, 4.37.

Preparation of 4b. A solution of **3b** (328 mg, 1.24 mmol) and 1.0 mL of cyclopentadiene (12.4 mmol) in 80 mL of hexane was irradiated for 5 h. The reaction was monitored by IR spectroscopy. The solution was concentrated in vacuo and chromatographed on alumina. After elution of a first yellow band with **3b** an orange elutate with **4b** and **1b** was collected. Crystallization at −80 °C and a second chromatography at −20 °C yielded **4b** (169 mg, 46%).

4b: sensitive brown powder; MS m/z (I_{rel}) 318 (39, M^+), 290 (100, $M^+ -$ CO); IR (hexane, cm^{-1}) 1979 s, 1977 s; ^{1}H NMR (C_6D_6) δ 8.05 (m, 2 H_o), 7.48 (m, 2 $H_m + H_p$), borole 2.59 (s, 2-/5-H) and 1.53 (s, 3-/4-Me), C_5H_6 4.90 (m, 2-/3-H), 2.87 (m, 1-/4-H), 2.09 (dm, ^2J = 14 Hz, 5endo-H), and 1.48 (d, ^2J = 14 Hz, 5exo-H); ^{11}B NMR ($CDCl_3$) δ 15.3.

Preparation of 1b. A solution of **3b** (2.10 g, 6.8 mmol) and 6.2 mL (75.8 mmol) of cyclopentadiene in 150 mL of hexane was irradiated for 14 h. The reaction was monitored by IR spectroscopy. After filtration and concentration in vacuo crystallization at −30 °C gave **1b** (1.15 g, 58%).

1b: very air-sensitive orange-red crystals; mp 46 °C dec; MS m/z (I_{rel}) 290 (100, M^+), 212 (100, $M^+ - C_6H_6$); ^{1}H NMR (toluene-d_8, −70 °C) δ 7.87 (m, 2 H_o), 7.31 (m, 2 $H_m + H_p$), 3.66 (s, Cp), borole 2.76 (s br (6.5 Hz), 2-/5-H), 1.90 (s, 3-/4-Me), and −5.56 (s br (8.7 Hz), FeH); ^{1}H NMR (toluene-d_8, 32 °C) δ 7.77 (m, 2 H_o), 7.28 (m, 2 $H_m + H_p$), 3.84 (s, Cp), borole 2.48 (s br (17 Hz), 2-/5-H) and 1.98 (s, 3-/4-Me), −5.25 (s br (30 Hz), FeH); in a spin saturation transfer experiment, homodecoupling at δ −5.25 results in intensity decrease at δ 2.48; ^{1}H NMR (toluene-d_8, 110 °C) δ 7.61 (m, 2 H_o), 7.17 (m, 2 $H_m + H_p$), 3.91 (s, Cp), borole + hydride 2.03 (s, 3-/4-Me) and −0.21 (s br (27 Hz), 2-/5-H + FeH); ^{11}B NMR ($CDCl_3$) δ =6.8; ^{13}C NMR (toluene-d_8, −65 °C) δ 138.7 (s, C_i), 134.8 (d, ^1J = 158 Hz, 2 C_o), 127.4 (d, ^1J = 158 Hz, 2 C_m), 126.5 (d, ^1J = 160 Hz, C_p), 76.4 (d, ^1J = 170 Hz, Cp), borole 108.2 (s, C-3/-4), 68.4 (d, ^1J = 153 Hz, C-2/-5), and 17.5 (q, ^1J = 126 Hz, 3-/4-Me); ^{13}C NMR (toluene-d_8, 27 °C) δ 135.0 (d, ^1J = 159 Hz, 2 C_o), 127.5 (d, ^1J = 158 Hz, 2 C_m), 126.5 (d, ^1J = 160 Hz, C_p), 76.2 (d, ^1J = 170 Hz, Cp), borole 107.6 (s, C-3/4), 68.0 (d br, C-2/5), and 17.2 (q, ^1J = 126 Hz, 3-/4-Me). Anal. Calcd for $C_{17}H_{19}BFe$: C, 70.41; H, 6.60. Found: C, 70.14; H, 6.56.

Preparation of 1e. By the same method **3a**[13] (2.60 g, 9.30 mmol) and 9.3 mL (93 mmol) of methylcyclopentadiene gave **1e** (1.04 g, 40%).

1e: red-brown powder, mp 31 °C dec; thermally labile, very sensitive to air and moisture; MS m/z (I_{rel}) 276 (94%, M^+), 198 (100, $M^+ - C_6H_6$), 170 (14, 198 − C_2H_2); ^{1}H NMR (C_6D_6) δ 7.90 (m, 2 H_o), 7.34 (m, 2 $H_m + H_p$), borole 5.32 (s br (7 Hz), 3-/4-H) and 2.65 (s br (13 Hz), 2-/5-H), C_5H_4Me 3.92 (s, 4 H) and 1.46 (s, Me), −4.44 (s br (22 Hz), FeH); ^{11}B NMR (C_6D_6) δ −5.5; ^{13}C NMR (C_6D_6) δ 135.6 (d, ^1J = 155 Hz, 2 C_o), signals of C_m and C_p hidden, borole 91.6 (d, ^1J = 167 Hz, C-3/-4) and 67.2 (d br, C-2/-5), C_5H_4Me 75.5 (d, ^1J = 173 Hz, C-3/-4), 73.4 (d, ^1J = 178, C-2/-5), and 14.4 (q, ^1J = 128 Hz, Me).

Preparation of 1c,d,f. To a solution of **1a,b,e** (2.00 mmol) in 50 mL of THF were added iodomethane (0.37 mL, 6.00 mmol) and an excess of NaH. The solution was stirred until the evolution of gas ceased (12 h). Removal of the solvent, extraction of the residue with hexane, filtration through alumina, and crystallization from a concentrated solution at −78 °C afforded the product.

1c: red, air-stable crystals (44%); mp 82 °C; dec pt >160 °C; MS m/z (I_{rel}) 290 (100, M^+), 274 (94, $M^+ - CH_4$), 212 (94, $M^+ - C_6H_6$); ^{1}H NMR (toluene-d_8, −80 °C) δ 8.04 (m, 2 H_o), 7.49 (m, 2 $H_m + H_p$), 3.66 (s, Cp), borole 4.94 (s, 3-/4-H) and 1.45 (s, 2-/5-Me), −5.78 (s br (5 Hz), FeH); ^{1}H NMR (toluene-d_8, 32 °C) δ 7.82 (m, 2 H_o), 7.38 (m, 2 $H_m + H_p$), 3.96 (s, Cp), borole 5.08 (s, 3-/4-H) and 1.37 (s, 2-/5-Me), −5.74 (s br (15 Hz), FeH); ^{1}H NMR (toluene-d_8, 110 °C) δ 7.81 (m, 2 H_o), 7.34 (m, 2 $H_m + H_p$), 4.08 (s, 3-/4-H + Cp), 1.35 (s, 2-/5-Me), −5.70 (s br (40 Hz), Fe H); ^{11}B NMR ($CDCl_3$) δ −8.6; ^{13}C NMR (CD_2Cl_2, −80 °C) δ 140.4 (s, C_i), 135.5 (d, ^1J = 155 Hz, 2 C_o), 127.9 (d, ^1J = 157 Hz, 2 C_m), 126.5 (d, ^1J = 159 Hz, C_p), 75.7 (dm, ^1J = 179 Hz, Cp), borole 89.3 (d, ^1J = 165 Hz, C-3/-4), 88.4 (s, C-2/-5), 18.0 (q, ^1J = 125 Hz, 2-/5-Me); ^{13}C NMR (CD_2Cl_2, 20 °C) δ 135.7 (d, ^1J = 155 Hz, 2 C_o), 127.8 (d, ^1J = 164 Hz, 2 C_m), 126.3 (d, ^1J = 159 Hz, C_p), 75.7 (dm, ^1J = 178 Hz, Cp), borole 89.7 (s, C-3/-4), 17.7 (q, ^1J = 126 Hz, 2-/5-Me). Anal. Calcd for $C_{19}H_{23}BFe$: C, 70.41; H, 6.60. Found: C, 70.01; H, 6.79.

1d: red air-stable crystals (89%); mp 104 °C; dec pt >180 °C; MS m/z (I_{rel}) 318 (85, M^+), 302 (58, $M^+ - CH_4$), 240 (100, $M^+ - C_6H_6$); ^{1}H NMR (toluene-d_8, −75 °C) δ 7.96 (m, 2 H_o), 7.22 (m, 2 $H_m + H_p$), 3.48 (s, Cp), borole 1.77 (s, 3-/4-Me), 1.34 (s, 2-/5-Me), and −6.58 (s br (7 Hz), FeH); ^{1}H NMR (toluene-d_8, 20 °C) δ 7.86 (m, 2 H_o), 7.19 (m, 2 $H_m + H_p$), 3.71 (s, Cp), borole 1.91 (s, 3-/4-Me) and 1.31 (s, 2-/5-Me), −6.49 (s br (15 Hz), FeH); ^{1}H NMR (toluene-d_8, 110 °C) δ 7.78 (m, 2 H_o), 7.19 (m, 2 $H_m + H_p$), 3.82 (s, Cp), borole 2.01 (s, 3-/4-Me) and 1.30 (s, 2-/5-Me), −6.43 (s br (37 Hz), FeH); ^{11}B NMR ($CDCl_3$) δ −8.7; ^{13}C NMR (CD_2Cl_2, −80 °C) δ 140.9 (s, C_i), 135.7 (d, ^1J = 155 Hz, 2 C_o), 127.9 (d, ^1J = 157 Hz, 2 C_m), 126.3 (d, ^1J = 159 Hz, C_p), 77.3 (dm, ^1J = 178 Hz, Cp), borole 105.1 (s, C-3/-4), 84.4 (s, C-2/-5), 15.3 (q, ^1J = 125 Hz, 2 Me), and 13.7 (q, ^1J = 126 Hz, 2 Me); ^{13}C NMR (CD_2Cl_2, 20 °C) δ 136.0 (d, ^1J = 155 Hz, 2 C_o), 127.7 (d, ^1J = 156 Hz, 2 C_m), 126.1 (d, ^1J = 159 Hz, C_p), 77.4 (dm, ^1J = 178 Hz, Cp), borole 105.2 (s, C-3/-4), 15.0 (q, ^1J = 125 Hz, 2 Me), and 13.4 (q, ^1J = 126 Hz, 2 Me). Anal. Calcd for $C_{19}H_{23}BFe$: C, 71.75; H, 7.23. Found: C, 71.66; H, 7.30.

1f: red, air-stable crystals (78%); mp 51 °C dec; MS *m/z* (I_{rel}) 304 (100, M^+), 288 (96, $M^+ - CH_4$), 273 (38, 288 − Me), 226 (95, $M^+ - C_6H_6$), 224 (93, $M^+ - C_5H_5Me$), 211 (47, 226 − Me), 209 (33, 211 − H_2), 144 (32, $C_6H_5BFe^+$), 132 (32, $C_5H_5BFe^+$); ^{1}H NMR ($CDCl_3$) δ 7.67 (m, 2 H_o), 7.28 (m, 2 $H_m + H_p$), borole 5.32 (s, 3-/4-H) and 1.38 (s, 2-/5-Me), C_5H_4Me 4.31 (s, 4 H) and 1.91 (s, Me), −5.79 (s br (14 Hz), FeH); ^{11}B NMR ($CDCl_3$) δ −8.0; ^{13}C NMR ($CDCl_3$) δ 135.3 (d, ^1J = 162 Hz, 2 C_o), 127.4 (d, ^1J = 157 Hz, 2 C_m), 125.9 (d, ^1J = 155 Hz, C_p), borole 90.3 (d, ^1J = 164 Hz, C-3/-4) and 17.2 (q, ^1J = 125 Hz, 2-/5-Me), C_5H_4Me 76.0 (C-3/-4), 74.3 (d, ^1J = 177 Hz, C-2/-5), and 14.2 (q, ^1J = 129 Hz, Me). Anal. Calcd for $C_{20}H_{26}BFe$: C, 71.11; H, 6.96. Found: C, 71.01; H, 7.06.

Preparation of 1g. NaH (0.150 g, 6.25 mmol) was added to a solution of **1a** (0.261 g, 1.00 mmol) in 40 mL of THF. After the mixture was stirred for 15 min at room temperature, 6-iodo-1-hexene (0.464 g, 2.20 mmol) was added and stirring was continued for 72 h. The solvent was removed, and the red residue was dissolved in Et_2O. Filtration and chromatography on alumina (20-cm column) gave a red band with **1g** (0.264 g, 62%), which was isolated by removing the solvent.

1g: red, slightly air-sensitive oil; MS *m/z* (I_{rel}) 426 (100, M^+); ^{1}H NMR (C_6D_6) δ 7.82 (m, 2 H_o), 7.36 (m, 2 $H_m + H_p$), 4.08 (s, Cp), borole 5.18 (s, 3-/4-H), hexenyl 5.4–6.0 (m, 2 5-H), 4.7–5.2 (m, 4 6-H), and 0.76–2.34 (m, 8 CH_2), −6.13 (s br (11 Hz), FeH); ^{11}B NMR (C_6D_6) δ −5.6; ^{13}C NMR (C_6D_6) δ 135.8 (d, ^1J = 155 Hz, 2 C_o), 127.6 (d, ^1J = 156 Hz, 2 C_m), signal of C_p hidden, 74.9 (d, ^1J = 178 Hz, Cp), borole 94.4 (s br (125 Hz), C-2/-5) and 88.0 (d, ^1J = 164 Hz, C-3/-4), hexenyl 139.1 (d, ^1J = 150 Hz, C-5), 114.4 (t, ^1J = 155 Hz, C-6), 33.8 (t, ^1J = 125 Hz, C-4), 32.0 (t, ^1J = 123 Hz, C-1), 31.9 (t, ^1J = 126 Hz, C-3), and 30.9 (t, ^1J = 124 Hz, C-2).

Preparation of 1h. As described above, **1a** (0.461 g, 1.77 mmol) in 25 mL of THF was stirred with NaH and (iodomethyl)-cyclopropane for 96 h. Chromatographic workup first gave a red band with 15 mg of an unidentified product that did not exhibit allylic NMR signals and then second a red band with **1h** (0.30 g, 46%).

1h: red, slightly air-sensitive oil; MS *m/z* (I_{rel}) 370 (100, M^+); ^{1}H NMR (C_6D_6) δ 7.90 (m, 2 H_o), 7.40 (m, 2 $H_m + H_p$), 4.06 (s, Cp), borole 5.35 (s, 3-/4-H), $(CH_2)_2CHCH_2$ 1.75 (dd, $^2J_{AB}$ = 15.5 Hz, $^3J_{A2}$ = 6.8 Hz, 1-H_A), 1.50 (dd, $^2J_{AB}$ = 15.5 Hz, $^3J_{B2}$ = 6.8 Hz, 1-H_B), and −0.3 to +0.5 (m, $(CH_2)_2CH$), −6.1 (s br (11 Hz), FeH); ^{11}B NMR (C_6D_6), δ −7.1; ^{13}C NMR (C_6D_6) δ 135.6 (d, ^1J = 155 Hz, 2 C_o), 125.8 (C_p), signal of C_m hidden, 74.6 (d, ^1J = 178 Hz, Cp), borole 93.5 (s br (70 Hz), C-2/-5) and 87.6 (d, ^1J = 164 Hz, C-3/-4), $(CH_2)_2CHCH_2$ 36.5 (t, ^1J = 125 Hz, 2 C-1), 11.6 (d, ^1J = 160 Hz, 2 C-2), 5.0 (t, ^1J = 160 Hz, 2 C-3), and 4.5 (t, ^1J = 161 Hz, C-3′).

Reaction of 1a with 1 Equiv of CNBu^t. NMR Experiment. CNBu^t (97 μL, 0.86 mmol) was added to **1a** (0.209 g, 0.80 mmol) in 2 mL of C_6D_6. The solution was kept at room temperature for 18 h while the reaction was monitored by NMR spectroscopy; the four compounds **1a** (29% of total of iron complexes), **9a** (53%), **11a** (18%), and free cyclopentadiene (amount approximately equivalent to **11a**) that of were observed.

9a: ^{1}H NMR (C_6D_6) δ 7.52 (m, 2 H_o), 7.22 (m, 2 $H_m + H_p$), 3.98 (s, Cp), C_4H_5B 5.98 ("t", $^3J_{34} = {}^3J_{23}$ = 4.1 Hz, 3-H), 4.53 (dd, $^3J_{23}$ = 4.1, $^4J_{24}$ = 1.9 Hz, 2-H), 4.00 (m, partly hidden by Cp signal), 4-H), 1.60 (d, $^2J_{5endo,5exo}$ = 15.7 Hz, 5endo-H), and 1.31 (d, $^2J_{5exo,5endo}$ = 15.7 Hz, 5exo-H), 0.93 (s, Bu^t); ^{11}B NMR (C_6D_6) δ 35.8; ^{13}C NMR (C_6D_6) δ 178.7 (s, CN), 135.3 (d, ^1J = 155 Hz, 2 C_o), signals of C_m and C_p hidden, 76.5 (d, ^1J = 176 Hz, Cp), C_4H_5B 92.1 (d, ^1J = 164 Hz, C-3), 59.9 (d, ^1J = 162 Hz, C-4), and C-2 and C-5 not observed, 56.1 (s, *C*Me$_3$), 30.5 (q, ^1J = 128 Hz, C*Me*$_3$).

Preparation of 11a. CNBu^t (0.22 mL, 1.93 mmol) was added to a solution of **1a** (0.480 g, 1.84 mmol) in Et_2O at 0 °C. After the reaction mixture was stirred for 15 h at room temperature, the volatiles were removed in vacuo. Chromatography of the residue on alumina (20-cm column) with hexane/Et_2O (8/1) gave a red band of **1a** (0.23 g, 50%) and a yellow band of **11a** (0.134 g, 17%).

11a: red, air-stable crystals; mp 88 °C; dec pt >220 °C; MS *m/z* (I_{rel}) 445 (80, M^+), 362 (96, M^+ − CNBu^t), 306 (82, 362 − C_4H_8), 279 (82, M^+ − 2 CNBu^t), 250 (67, 362 − 2 C_4H_8), 223 (100, 279 − C_4H_8), 196 (82, M^+ − 3 CNBu^t); IR (Et_2O, cm^{-1}) 2126 s (CN), 2046 vs; ^{1}H NMR (CD_3COCD_3) δ 7.61–7.48 (m, 2 H_o), 7.22–7.07 (m, 2 $H_m + H_p$), borole 4.58 (m, $^3J + {}^4J$ = 5.9 Hz, 3-/4-H) and 2.83 (m, $^3J + {}^4J$ = 5.9 Hz, 2-/5-H), 1.27 (s, 3 Bu^t); ^{11}B NMR (CD_3COCD_3) δ 15.7; ^{13}C NMR (CD_3COCD_3) δ 179.2 (s, 3 CN), 135.2 (d, ^1J = 154 Hz, 2 C_o), 127.6 (d, ^1J = 155 Hz, 2 C_m), 126.2 (d, ^1J = 158 Hz, C_p), borole 88.1 (d, ^1J = 165 Hz, C-3/-4) and 68.7 (d br, ^1J = 158 Hz, C-2/-5), 56.9 (s, 3 *C*Me$_3$), 31.5 (q, ^1J = 128 Hz, 3 C*Me*$_3$). Anal. Calcd for $C_{25}H_{36}N_3BFe$: C, 67.44; H, 8.15; N, 9.43. Found: C, 67.56; H, 8.12; N, 9.57.

Reaction of 1a-*d*$_3$ with CNBu^t. The NMR experiment described above for **1a** was repeated with **1a**-d_3. Isotopic purity of the complex products was estimated from intensities of residual proton signals.

9a-d_3: ^{1}H NMR (80 MHz, C_6D_6) C_4H_5B δ 6.01 (d, 4-H) and 4.03 (d, 3-H) as AB system with $^3J_{34}$ = 3.6 Hz, only residual intensity for signals at 4.53 (5-H), 1.60 (2endo-H) and 1.31 (2exo-H).

11a-d_2: ^{1}H NMR (80 MHz, C_6D_6) borole δ 5.07 (s, 3-/4-H), only residual intensity for 2-/5-H signal.

Reaction of 1a-*d*$_3$ with CNBu^t and Trapping of the Cyclopentadiene Formed. CNBu^t (1.0 mL, 8.8 mmol) was added to **1a**-d_3 (1.19 g, 4.5 mmol) in 20 mL of toluene. After the mixture was stirred at room temperature for 6 h, the volatiles were condensed into a cold flask (cooled by liquid nitrogen), containing maleic acid anhydride (0.33 g, 3.4 mmol). Then the flask was heated to reflux temperature for 3 h. Removal of the volatiles in vacuo left a white residue, which was examined by mass spectroscopy. The isotopic pattern at *m/z* 165 indicated 85% monodeuteration for the adduct **12**.

Preparation of 10. A mixture of Fe(CO)$_2$(CNBu^t)(C_4H_4BPh)[9] (0.900 g, 2.70 mmol) and cyclopentadiene (0.4 mL, 4 mmol) in 80 mL of hexane was irradiated at 0 °C to produce ca. 5 mmol of CO (200 min). The mixture was concentrated to 10 mL and cooled to −30 °C to give a brown powder (0.71 g) consisting of **13** (25%) and **10** (75%). Chromatography on alumina (20-cm column) with hexane at −30 °C yielded three bands, a yellow band of **13** (23%), a red band with **10** (25%), and a red band with **11a** (15%) resulting from decomposition of **10** on the column.

10: dec pt 90 °C; IR (toluene, cm^{-1}) 2112 s (CN), 2080 m; ^{1}H NMR (C_6D_6) δ 8.05 (m, 2 H_o), 7.38 (m, 2 $H_m + H_p$), borole 4.86 (m, 3-/4-H) and 2.77–2.64 (m, 2-/5-H and 1-/4-H of C_5H_6), C_5H_6 5.74 (m, 2-/3-H), 2.14 (dm, $^2J_{AB}$ = 12.3 Hz, 5-H_A), and 1.71 (dm, $^2J_{AB}$ = 12.3 Hz, 5-H_B), 1.00 (s, Bu^t); ^{11}B NMR (C_6D_6) δ 17.8; ^{13}C NMR (C_6D_6) δ 183.2 (s, CN), 135.4 (d, ^1J = 156 Hz, 2 C_o), signals of C_m and C_p hidden, borole 88.6 (d, ^1J = 164 Hz, C-3/-4) and 64.3 (d br, ^1J = 154 Hz, C-2/-5), C_5H_6 79.7 (d, ^1J = 175 Hz, C-2/-3), 57.5 (d, ^1J = 167 Hz, C-1/-4), and 42.0 (t, ^1J = 126 Hz, C-5), 56.7 (s, *C*Me$_3$), 30.2 (q, ^1J = 125 Hz, C*Me*$_3$).

Reaction of 10 with Excess CNBu^t. CNBu^t (20 μL, 180 μmol) was added to a solution of **10** (20 mg, 58 μmol) in 0.5 mL of C_6D_6. An instantaneous change of color from red to light orange occurred. The NMR spectrum of the reaction mixture showed complete conversion of **10** to **11a** and free cyclopentadiene.

Table 9. Crystallographic Data, Data Collection Parameters, and Refinement Parameters

	1d	1f
formula	$C_{19}H_{23}BFe$	$C_{18}H_{21}BFe$
fw	318.05	304.02
space group	$I4_1/a$ (No. 88)	$P2_1/n$ (No. 14)
a, pm	2806.1(4)	1180.9(2)
b, pm		844.3(1)
c, pm	824.5(2)	1577.8(1)
β, deg		102.11(1)
V, nm^3	6.491(2)	1.538(4)
Z	16	4
density (calc), g cm^{-3}	1.301	1.313
cryst size, mm^3	0.12 × 0.10 × 0.06	0.33 × 0.29 × 0.10
μ(Mo Kα), cm^{-1} [a]	0.91	0.97
radiation (λ, pm)	Mo Kα (71.069)	Mo Kα (71.069)
monochromator	graphite	graphite
temp, K	120	125
scan mode (2θ range, deg)	ω–2θ (3–50)	ω–2θ (3–50)
no. of unique rflns	2754	2721
N_o, no. of obsd rflns [b]	2187	2554
N_p, no. of params refined	167	209
R [c]	0.047	0.037
R_w [d]	0.042 [e]	0.039 [f]
residual electron density, 10^{-6} e pm^{-3}	0.51	0.54

[a] No corrections for absorption and extinction were applied. [b] $F_o \geq 4\sigma(F)$. [c] $R = \sum||F_o| - |F_c|| / \sum|F_o|$. [d] $R_w = [\sum w(|F_o| - |F_c|)^2 / \sum w|F_o|^2]^{1/2}$. [e] $w^{-1} = \sigma^2(F_o) + 0.000137F_o^2$. [f] $w^{-1} = \sigma^2(F_o) + 0.001F_o^2$.

Reaction of 1c with Excess CNBu^t. NMR Experiment. CNBu^t (40 μL, 360 μmol) was added to a solution of **1c** (35 mg, 120 μmol) in 0.5 mL of C_6D_6. The solution was kept at room temperature for 30 days; the reaction was monitored by NMR spectroscopy, finally giving **9c** (25%), **11c** (75%), and free cyclopentadiene (amount approximately equivalent to that of **11c**).

9c: ^{1}H NMR (C_6D_6) δ 7.89 (m, 2 H_o), 7.39 (m, 2 H_m + H_p), 3.81 (s, Cp), C_4H_5B 5.07 (d, 3-H) and 4.81 (d, 4-H) as AB system with $^3J_{34}$ = 3.9 Hz, 2.16 (s, 2-Me), 1.83 (s, 5-Me), and 1.35 (s, 5-H), 0.88 (s, Bu^t).

11c: ^{1}H NMR (C_6D_6) δ 8.18–8.06 (m, 2 H_o), 7.55–7.23 (m, 2 H_m + H_p), borole 4.68 (s, 3-/4-H) and 2.00 (s, 2-/5-Me), 1.04 (s, Bu^t).

Crystal Structure Analysis of 1d and 1f. Suitable crystals of **1d** and **1f** were obtained from concentrated hexane solutions at low temperatures (−78 °C). Pertinent crystallographic data are collected in Table 9.

Electrochemical Procedures. Cyclic voltammograms were measured using a Princeton Applied Research (PAR), EG&G) Model 173 potentiostat and Model 175 function generator, a Metrohm electrochemical cell, and Metrohm platinum-disk electrodes. Moderate sweep rate cyclic voltammograms were recorded on a Houston Instrument Series 2000 X-Y recorder, and rapid scan rate data were obtained on a Hameg HM 208 two-channel storage oscilloscope. All potentials are given in V vs a SCE as reference electrode that was equipped with a salt bridge (Metrohm) of composition identical with that of the investigated solution. Ferrocene was used for calibration and as an internal standard. Purification of electrolytes and solvents and cell measurements were conducted under argon. Bu_4NPF_6 (Fluka electrochemical reagent grade) was dried at 110 °C for 20 h in vacuo before use. DME (Aldrich 99+%) was passed through a column of activated basic alumina (ICN Alumina B Super I, activated at 280 °C for 2 days in vacuo) and distilled twice before use. The solvent was stored under argon, and freshly prepared solutions of electrolytes were stored in Schlenk tubes equipped with Teflon valves.

EPR and Paramagnetic NMR Measurements. Pure solutions of [Li(TMEDA)]**5a**[9] in THF-d_8 allow the observation of diamagnetic NMR spectra (f_p = 0). Stepwise oxidation was performed in the NMR tube by briefly exposing the solution to air and subsequent strong shaking. This procedure yields **5a**/**5a**$^-$ mixtures with increasing contents of **5a**. For complete oxidation (f_p = 1) an excess of oxygen and strong shaking is required. This sample was also used for the EPR measurement after cooling to 100 K. To prove the chemical reversibility of the oxidation, a second sample of partly oxidized [Li(TMEDA)]**5a** was prepared in THF-d_8. The sample tube was fitted with a potassium mirror at the top and sealed. Reduction was performed by turning the tube upside down several times. Again a series of NMR spectra are obtained which fit perfectly to the data of the oxidation experiment. This method has been employed previously in the ^{1}H NMR characterization of paramagnetic multidecker sandwich and metallacarborane complexes.[24] The paramagnetic mole fractions f_p are determined via the linearity of δ_{obs} (Figure 9).

Acknowledgment. We thank the Deutsche Forschungsgemeinschaft and the Fonds der Chemischen Industrie for generous support of this work and an FCI graduate fellowship for T.C.

Supplementary Material Available: Tables of crystal data and structure solution and refinement details, bond distances and angles, anisotropic thermal parameters, and hydrogen atom coordinates for **1d** and **1f** (14 pages). Ordering information is given on any current masthead page.

OM930511C